Surface-oxygen induced electrochemical self-assembly of mesoporous conducting polymers for electrocatalysis

Journal:	*Journal of The Electrochemical Society*
Manuscript ID	JES-101393.R1
Manuscript Type:	Research Paper
Date Submitted by the Author:	13-Jun-2020
Complete List of Authors:	Lahiri, Abhishek; Brunel University London, Department of Chemical Engineering Chutia, Arunabhiram; University of Lincoln - Brayford Campus Carstens, Timo; Clausthal University of Technology, Institute of Electrochemistry Endres, Frank; Tech Univ Clausthal, Electrochemistry
Keywords:	Electrocatalysis, Ionic liquids, Water splitting, Electropolymerization, Conducting polymers, Self Assembly, DFT

SCHOLARONE™
Manuscripts

Accepted Manuscript

Surface-Oxygen Induced Electrochemical Self-Assembly of Mesoporous Conducting Polymers for Electrocatalysis

Abhishek Lahiri,[1, 2*] Arunabhiram Chutia,[3, 4,z] Timo Carstens,[1] and Frank Endres[1,z]

[1]Institute of Electrochemistry, Clausthal University of Technology, 38678 Clausthal-Zellerfeld, Germany

[2]Department of Chemical Engineering, Brunel University London, London UB8 3PH, UK

[3]School of Chemistry, Brayford Pool, University of Lincoln, Lincoln, LN6 7TS, UK

[4]UK Catalysis Hub, Research Complex at Harwell, Rutherford Appleton Laboratory, Harwell, Oxon OX11 0FA, United Kingdom

[z]E-mail: abhishek.lahiri@brunel.ac.uk; achutia@lincoln.ac.uk; frank.endres@tu-clausthal.de

Abstract

Porous polymers have immense potential in catalysis, energy conversion and storage, separation sciences and life sciences due to their high surface area and high diffusion flux. Developing porous polymers with micro and mesoscale porosity with long-range order is challenging and involves multistep templated approaches. Here we demonstrate a simple surface-oxygen induced electropolymerization route to directly obtain self-assembled porous polymers of polyparaphenylene (PPP) and PPP based copolymers in ionic liquids. By combining experimental and theoretical studies, we show that surface oxygen on Cu changes the orientation and assembly of benzene which then results in a change in electropolymerization mechanism leading to a self-assembled porous structure with porosity between 2 and 5 µm. Furthermore, with controlled experimental parameters, bicontinuous conducting polymers with porosity of >10 µm are obtained. The porous conducting polymers show absorption of light in the visible range which was also used as an efficient electrode for investigation of the photo/electrochemical oxygen evolution reaction.

Introduction

Synthesis of porous polymer thin films by phase separation generally requires the polymer to be dissolved in a volatile solvent which on evaporation leads to direct formation of interconnected

Accepted Manuscript

For Peer Review Only

porous structures [1-4]. The phase separation of the polymer mixtures mainly depends on temperature and composition. However, it has also been shown that the presence of a surface on which the thin films are grown plays a significant role which defines the phase separation/deposition process as well as the crystallographic orientation of the polymer film.[5-7] Alternatively, a sacrificial template-assisted technique is a versatile route for developing a range of macroporous polymers by self-assembly or by electropolymerization[8-10]. However, after the polymerization process, the sacrificial template has to be chemically removed to obtain the macroporous polymer structures, which can also damage the polymer structure. Interfacial polymerization, which includes microemulsion media is another route for developing porous polymers. The major constrain in microemulsion media is the choice of monomers and reaction conditions, which has to be maintained to confine the polymerization to the interface.[10, 11] Therefore, further developments are desirable to reduce additional processing and reaction conditions to directly obtain porous polymers.

The effect of a substrate in the formation of patterned polymer films has been limited to studying phase separation phenomena. [4, 5, 12] Little has been investigated regarding the growth of polymer films directly on different substrates. For example, using vapour deposition of polymers, it was shown that the presence of surface oxygen on metals affects the wettability, which then leads to rectangular crystallite structures of the polymer.[7, 13, 14] In comparison however, deposition on the same metal without surface oxygen leads to a well ordered structure. This was recently shown to be due to van der Waals forces induced reconstruction of the polymer layer at the metal/polymer interface.[14] In comparison to phase separation and vapour deposition, in electropolymerization the surface-wetting changes with applied electrode potential and might lead to various nanostructures including porous structures, which are yet to be explored. Furthermore, although electropolymerization has been used to synthesize various polymer thin films including template-assisted porous structures, studies have been limited to growing the polymers on inert electrodes such as graphite or Pt as they do not undergo electrodissolution at anodic potentials.[15, 16] Unlike aqueous and organic solutions, ionic liquid electrolytes with a stable anion can in-effect impede the corrosion/electrodissolution issue at oxidative potentials and thereby promote the electropolymerization of different polymers having different microstructures.

Here we show an electrochemical self-assembled phenomena during electropolymerization of benzene in 1-hexyl-3-methylimidazolium tris(pentafluoroethyl)trifluorophosphate [HMIM]FAP

Accepted Manuscript
For Review Only

ionic liquid wherein porous polymers are obtained on oxidized copper whereas deposition on copper metal led to non-porous thin films. Theoretical studies show that the oxygen on copper influences the orientation of benzene on the substrate leading to a self-assembled porous structure. This technique is further exploited to deposit benzene-based-copolymers with varying porosity showing the possibility to apply this technique to develop other polymers. Finally, the polymer is tested for oxygen evolution reaction which shows highly efficient catalytic performance.

Results and Discussion

We first test the oxidation potential of the ionic liquid [HMIM]FAP on Cu to determine the possibility of depositing the polymer without copper dissolution (Figure S1). In the oxidation potential regime, a small oxidation peak is observed at 2.5 V followed by an increase in current to 3 V. The current for the first oxidation process is low (25 µA), which suggests adsorption/interfacial processes of the ionic liquid on copper. The increase in current beyond 2.5 V might be related to the decomposition of the FAP anion. Therefore, from ionic liquids with FAP ion, it is possible to synthesize different polymers if the polymerization process occurs below 2.5 V.

Figure 1 shows the cyclic voltammetry of the electropolymerization of benzene in [HMIM]FAP on different substrates. On Pt (Figure 1a) the first cyclic voltammetry (CV) cycle shows an increase in current at a potential of ~1.6 V, which is related to the electropolymerization of benzene. In subsequent cycles, polymerization begins at ~1.75 V. Similar CV curves for the polymerization of benzene are observed on Au (Figure 1b) wherein polymerization commences at ~1.5 V in the first cycle and shifts to ~1.9 V in subsequent cycles.

Accepted Manuscript
For Review Only

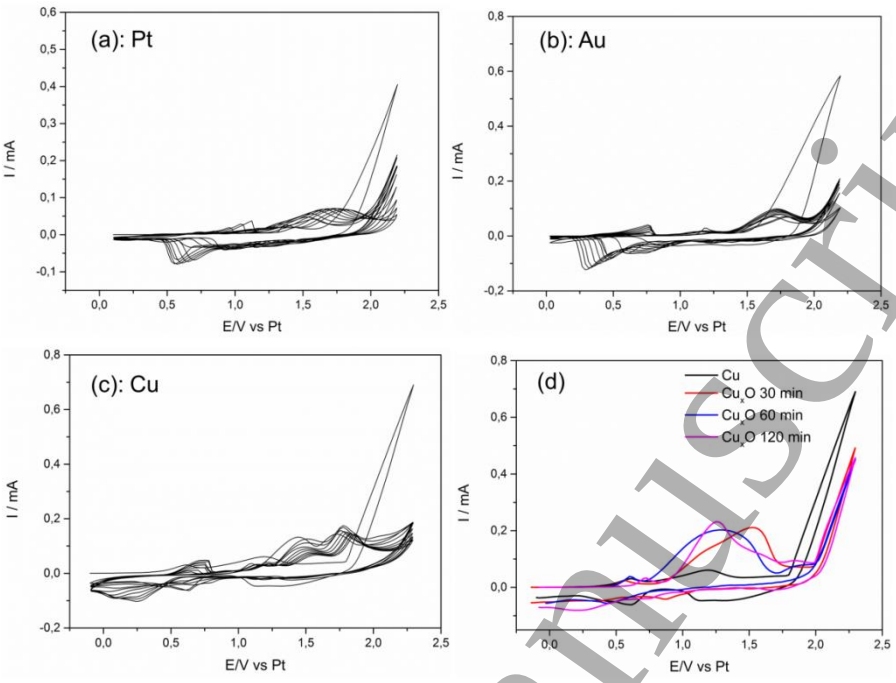

Figure 1: Cyclic voltammetry of 0.1M Benzene in [HMIM]FAP (a) Pt (b) Au (c) Cu and (d) Cu and Cu_xO

On Cu, the CV curves show a similar behavior like on Pt and Au wherein electropolymerization of benzene commences ~1.75 V for the first cycle and shifts to ~2.0 V in subsequent cycles. The presence of oxygen on Cu changes the electrochemical oxidation behavior completely. Figure 1d compares the first CV cycle of the electropolymerization of benzene on Cu and Cu_xO (see experimental section for Cu_xO characterization). The presence of oxygen on copper results in a first broad oxidation peak centered at ~1.3 V to ~1.5 V followed by an increase in current from ~1.75 V. The first oxidation peak can be attributed to some surface processes related with interaction of benzene with Cu_xO which is then followed by polymerization of benzene at ~1.75 V. Repeated experiments showed that only the presence of oxygen on copper is responsible for the occurrence of the first peak seen in Figure 1d. Figure S2 shows 10 representative CV cycles of 0.1M benzene in [HMIM]FAP on Cu_xO. It is evident from the CV cycles (Figure S2) that the oxidation peak at ~1.3 V to ~1.5 V (in the first cycle) shifts to positive potentials with cycling.

Figure 2 shows the morphology of the polyparaphylene (PPP) obtained on different substrates. On both Pt and Au substrates (Figure 2a, 2b), a polymer thin film structure can be distinguished

Accepted Manuscript
For Review Only

with the presence of some dents. A similar PPP structure is seen on Cu wherein a few circular holes are present.

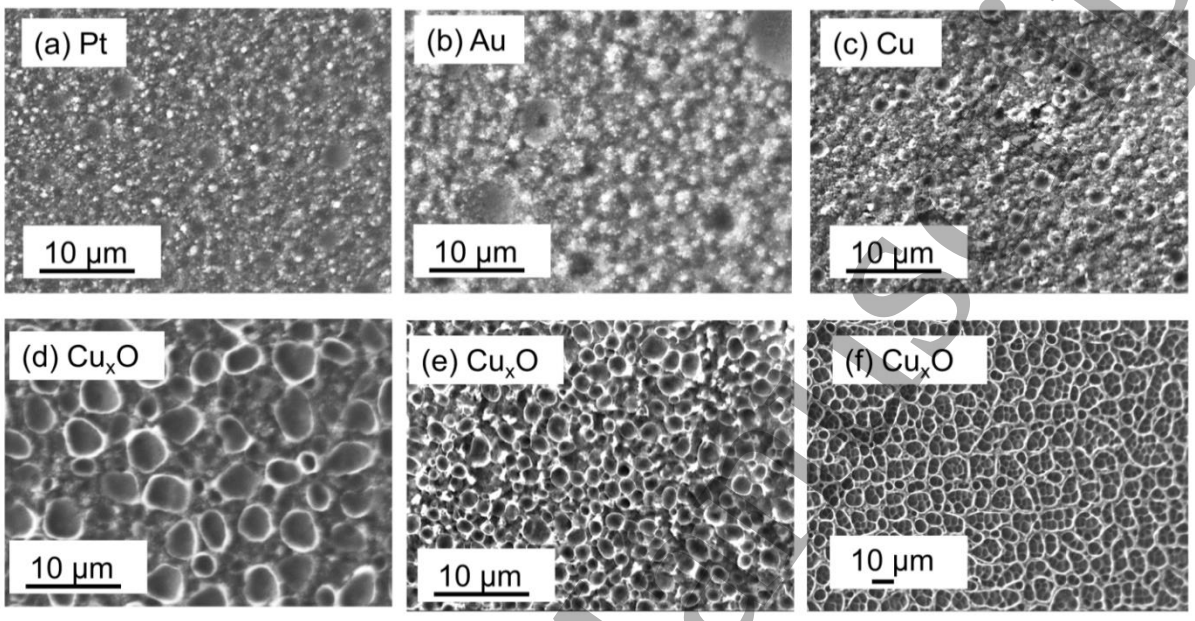

Figure 2: Microstructure of PPP on different substrates (a) Pt (b) Au (c) Cu and (d-f) Cu_xO

The high-resolution image of PPP in Figure S3a indicates that the holes might be some defects in the polymer thin film. However, on performing the deposition on Cu_xO, Figure 2 (d and e) shows the formation of pores between 0.1 and 6 µm (see pore size distribution plot in figure S3b). The high-resolution image in Figure S3c-e clearly demonstrates the microporous structure on exposing copper to oxygen. With controlled experimental parameters (see experimental section), interconnected porous PPP structures of >10 µm (figure 2f) can be obtained on Cu_xO substrates. Thus, based on the CV and polymer morphology it is evident that the presence of oxygen on the Cu substrate leads to the deposition of porous polymers. The possibility of electrochemical formation of porous polymers in ionic liquids can be due to either phase separation[17] or self-assembly. From in situ optical microscopic analysis, no liquid phase separation was observed. Therefore, the porous polymers can only be formed by self-assembly which was investigated using density functional theory calculations (DFT).

From in situ AFM studies it was observed that the electrode/electrolyte interface is dominated by C_6H_6 (see fig S4). For DFT, first the adsorption of C_6H_6 is systematically explored on different positions of Cu(111) and Cu_2O(111) surface (Figure S5 and S6) as it was observed

Accepted Manuscript - View Only

experimentally that C_6H_6 governs. It is evident that all the relaxed structures have similar final geometries for C_6H_6/Cu(111) systems and it is seen that the C_6H_6 molecule is weakly adsorbed on the Cu(111) surface with an adsorption energy (E_{ad}) ranging from -0.952 eV to -0.972 eV, which is considerably high as compared to its adsorption on the Cu_2O(111) surface (E_{ad} = -2.612 eV to -2.739 eV, Figure S6). A closer investigation on the geometry of the benzene molecule on the most stable C_6H_6/Cu(111) and C_6H_6/Cu_2O(111) reveal (see Figure 3 (a –b)) that in the former the nearest distance of C_6H_6 molecule from the surface of Cu(111) is ~2.783 Å and in the later it is 2.252 Å, which also reflects the fact that the benzene molecule is more strongly adsorbed on the Cu_2O(111) surface. On further examining the geometry of the adsorbed C_6H_6 molecule it is seen that in both the models the C_6H_6 molecule retained its planar geometry but on the Cu_2O(111) surface it attained a slanted orientation as opposed to the parallel orientation in the C_6H_6/Cu(111) models (Figure 3a, b). To better understand the underlying reason for the unique geometry of C_6H_6 on Cu(111) and Cu_2O(111) we analyze the Bader charges on the most stable configuration of these surfaces.

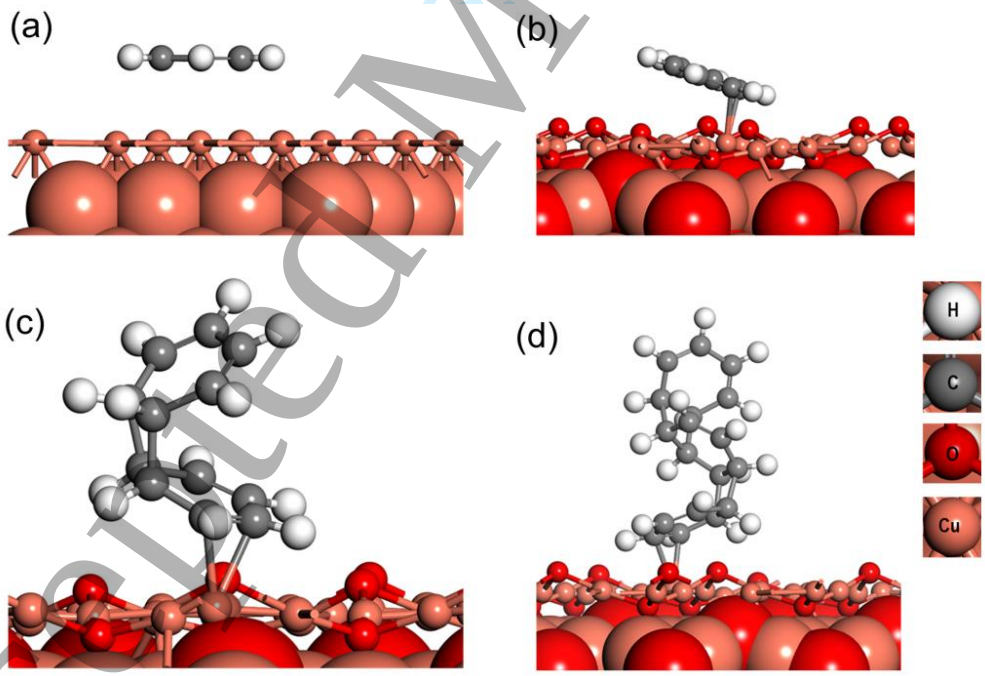

Figure 3. Optimised geometries of benzene on (a) Cu(111) and (b) Cu_2O(111) surfaces. ((c) and (d))The fully relaxed self-assembled structures of 2 and 3 molecules of benzene on Cu_2O(111) surface. For clarity, the benzene molecule(s) and the first atomic layer of the Cu(111) and Cu_2O(111) are represented as ball and stick and rest of the model is shown in CPK formalism.

Accepted Manuscript For Review

The calculated average Bader charge on the phenyl ring (C_{phe}) of the C_6H_6 molecule adsorbed on Cu(111) surface is found to be –0.075 e, and the charge distribution on the top layer of Cu-atoms showed a small residual charge of -0.020 e. The presence of a small negative charge on the phenyl ring and on the exposed Cu surface causes a weak electrostatic repulsion leading to physisorption of the C_6H_6 molecule on the Cu(111) surface. A similar analysis on C_6H_6/Cu_2O(111) system show that the exposed surface of Cu_2O(111) had positively and negatively charged centers of Cu and O ions with an average charge of +0.512 e and -0.948 e respectively. Further to this, the average charge on the C_{phe} ring is found to be -0.054 e meaning there is an attractive and repulsive interaction between positively charged Cu-ions and negatively charged O-ions respectively leading to a slanted geometry facilitated by the formation of a bond between a C-atom of C_6H_6 and Cu-atom of Cu_2O surface (Figure 3b)

Since the adsorption energy of the C_6H_6 molecule on the Cu_2O(111) surface is -1.766 eV lower than that on the Cu(111) surface, we further extend our studies on the adsorption of two and three molecules of C_6H_6 on the Cu_2O(111) surface. As shown in Figure S7, to understand the nature of the adsorption of two benzene molecules we consider three different models. In the first model, the two benzene molecules are placed one over the other (Figure S7a), in the second model we placed the second benzene on top of the adsorbed benzene in such a way that the C-atoms of the second C_6H_6 molecule are on the C–C bond of the adsorbed molecule (Figure S7b) and in the final model we place the second molecule parallel to the surface and away from the adsorbed C_6H_6 molecule (Figure S7c). Our calculations reveal that in the relaxed model-5 (Figure S7 (a)) the second benzene ring moved away from the first ring by a distance of 3.694 Å, which is close to the distance between graphene layers in graphite. In Model-6 (Figure S7 (b)), the C_6H_6 molecules self-assembled to form a fused structure of two C_6H_6 molecules (Figure 3(c)) and in Model-7 (Figure S7 (c)), both the C_6H_6 molecule adsorb on the Cu_2O(111) in a similar slanted fashion. From these analyses we conclude that based on the orientation of the C_6H_6 molecules on the Cu_2O, they may self-assemble to form fused structures and under potential the orientation of these molecules would change rendering the formation of a porous network structure. To further elucidate this fact, we consider Model-6 and Model-7 to adsorb a third C_6H_6 molecule and the fully relaxed structures are shown in Figure S8. The reason for such self-assembly can be ascribed to a free-radical-like reaction mechanism [18] i.e., in all our models the C_6H_6 molecules were adsorbed to the Cu_2O(111) surface by forming two bonds, leaving two extra electrons on

https://mc04.manuscriptcentral.com/jes-ecs

Accepted Manuscript For Review Only

the phenyl ring, which in turn initiate a chain reaction for the C_6H_6 molecular self-assembly. Based on these calculations, it can be inferred that the first oxidation peak in the CV of 0.1M Benzene in [HMIM]FAP on Cu_xO (figure 1d) might be related to surface processes which reorients the polymer chain and on applying more positive potential leads to a radical coupling reaction forming the porous PPP polymer.

Experiments with a lower number of CV cycles also show the formation of porous structures. Figure S9a shows the low- and high-resolution images of PPP after three CV cycles wherein pore size distribution of 0.5-6 μm (figure S9b) is evident, which agrees with the DFT calculations. With cycling, the deposition takes place over the porous structure and the polymer thickness increases. The same technique is also used to obtain copolymers of PPP and polythiophene (Figure S10 and S11), which show a porous network structure on Cu_xO whereas a non-porous structure on Au, thus showing that this technique is not limited to developing a single polymer but can be exploited to develop other copolymers.

As the electropolymerization depends on the substrate, FTIR is used to evaluate the changes in the polymer film and to calculate the degree of polymerisation. Figure 4 (a) compares the FTIR of PPP obtained on different substrates. Peaks related to aromatic ring, in-plane, out of plane and terminal C-H bonds are evident which are characteristic for the formation of PPP.[19, 20] A peak related to cross-linking is also observed at 1600 cm^{-1}.[21] However, it is evident that the intensity of the peaks varies with the substrate. The change in intensity of the terminal C-H and out of plane C-H bonds have been related to the change in the degree of polymerization [22] from which it can be inferred that the polymerization process changes on different substrates. The degree of polymerization was estimated from the ratio of the intensities of the absorption band of C-H out of plane vibrations of para (out of plane C-H bonds) and mono (terminal C-H bonds) substituted phenyl rings [22, 23].

The degree of polymerization for PPP deposited on Pt is found to be 14 whereas on Au, Cu and Cu_xO it is 17, 22 and 25, respectively, which evidences differences in the electropolymerization mechanism on different substrates. The survey spectra of the PPP on different substrates are shown in figure S12 wherein C 1s, O 1s and F 1s peaks are observed. The F1s peak arises from the FAP anion. Figure 4b shows the XPS C1s high resolution spectra of PPP deposited on different substrates. On Au, the asymmetric peak centered at 285.7 eV can be deconvoluted to

Accepted Manuscript For Review Only

four peaks. The peaks at 284.8, 286.0, 287.2 and 288.4 eV can be related to C-C, C-O, C=O and O-C=O respectively. [24] Two shake-up satellite peaks are observed at 290.5 and 293.4 eV, which indicate π-π* transitions in PPP valence electrons. [25] PPP deposited on Pt can be deconvoluted to four peaks at 284.8, 285.5, 286.8, 288.2 eV which can be related to similar C-C and C-O bonds as seen for PPP on Au. The slight shift in the binding energy can be ascribed to the new interfacial states that might have formed in the metal-PPP systems.[26-28] In the case of Cu and Cu_xO, the main C1s at 284.8 eV corresponding to C-C with a shoulder corresponding to C-O and C=O. However, the shake-up structures in case of Pt and Cu_xO are weak, which indicates a change in the electronic structure of PPP.

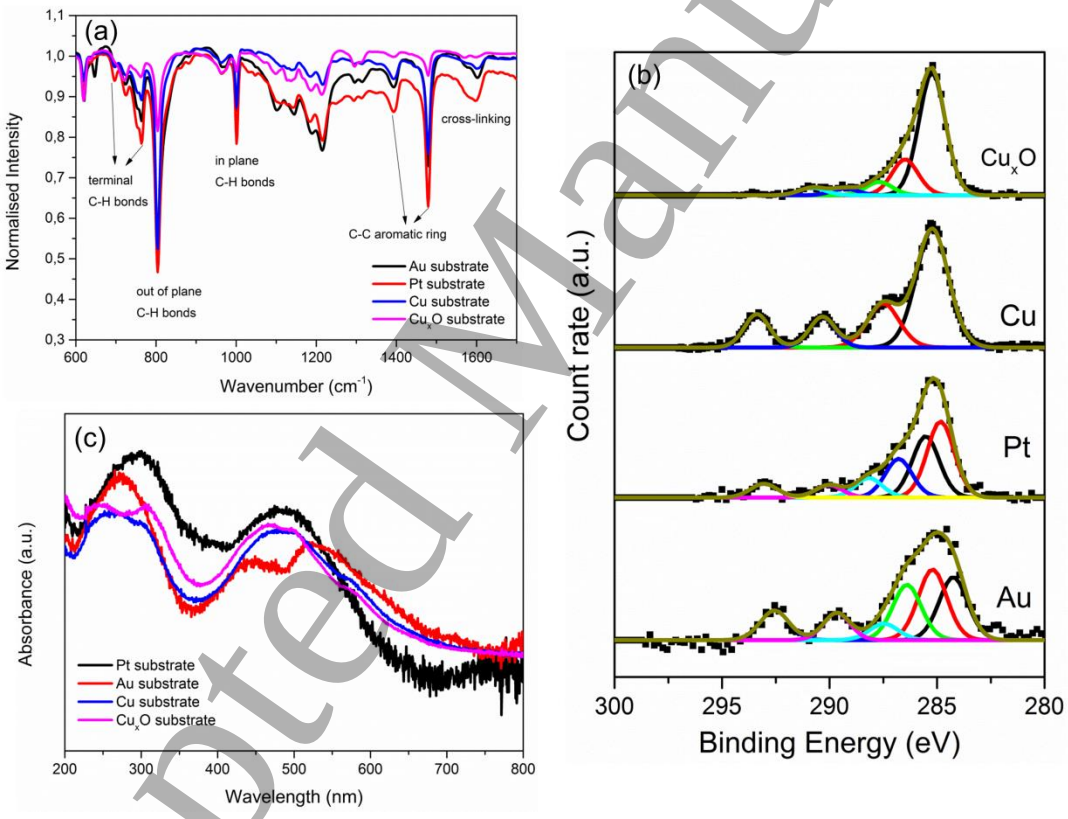

Fig 4: (a) FTIR of PPP on different substrates (b) C 1s high resolution XPS spectra of PPP on different substrates (c) UV vis spectra of PPP deposited on different substrates

UV visible spectroscopy of the polymer in Figure 4c show that PPP polymerized on Au gives rise to three peaks at 521, 446 and 272 nm, whereas PPP polymerized on Pt shows absorbance peaks at 486 and 298 nm. On Cu and Cu_xO, peaks at 485 and 264 nm and 485, 305 and 298 nm are observed, respectively. The difference in absorbance clearly results due to the change in the

Accepted Manuscript

electronic structure of the PPP. Furthermore, the PPP synthesized from the ionic liquid showed a clear red shift towards visible region compared to PPP synthesized using other techniques, which has been attributed to longer conjugated segments in the polymer [29-31]. Thus from FTIR, UV vis spectroscopy and XPS measurements, it is evident that the substrate affects the electropolymerization process, which is also supported by DFT calculations.

Finally, we tested the functional properties of the polymer for oxygen evolution reaction in an alkaline solution. As wettability affects the electrocatalytic process, the contact angle of KOH on the polymer was measured. Figure 5a shows that the contact angle of non-porous PPP deposited on Au has a contact angle of 117° whereas this decreases to 40° on porous PPP deposited on Cu_xO. In Figure 5b the linear sweep voltammetry of oxygen evolution reaction (OER) in 1M KOH is presented.

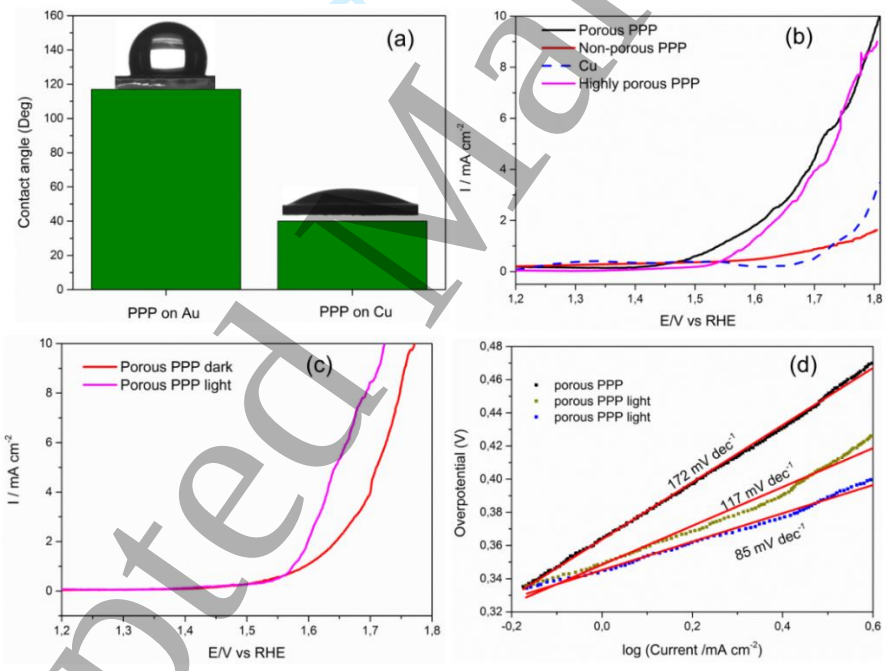

Fig 5: (a) Contact angle measurement on PPP electrodeposited on Au and Cu_xO (b) OER reaction on different PPP (c) OER reaction in dark and under illumination (d) Tafel slopes of OER reaction in dark and under illumination.

It is evident that the OER process on copper occurs at 1.7 V whereas for the non-porous PPP the OER commences around 1.6 V. However, the current density measured for the OER process in non-porous PPP is extremely low. In comparison, both porous PPP and bicontinuous PPP show a

Accepted Manuscript

good OER performance, which commences around 1.52 V and reaches a current density of 10 mA cm^{-2} at 1.81 V. Repeated experiments show that the potential needed to reach a current density of 10 mA cm^{-2} takes place between 1.75 and 1.82 V. The overpotential in porous PPP is between 520 and 590 mV from the thermodynamic potential and is better than graphene-based materials including C_3N_4 which has an overpotential of >700 mV to achieve the same current density. [31, 32] Furthermore, due to the visible region absorbance and a bandgap of 2.9 eV [33] of the polymer, OER was tested in the presence of 50 mW green LED. A change in slope is observed for the OER process and the current density of 10 mA cm^{-2} is achieved at a much lower overpotential of 470 mV (1.7 V vs RHE). This value is lower than IrO_2 which results in an overpotential of 510 mV to achieve the same current density. [32, 34] The Tafel plot in Figure 5d clearly shows that a much higher slope of 172 mV dec^{-1} is achieved for OER of PPP in dark whereas the slope decreases between 85 and 117 mV dec^{-1} under illumination.

Conclusion

In conclusion, we have shown a simple technique to obtain porous polymers using surface oxygen induced electrochemical self-assembly. The effect of substrate not only changes the morphology but also influences the electropolymerization process as well as the degree of polymerization. DFT calculations clearly show that the oxygen present on the metal influences the orientation of benzene, which then affects the electropolymerization process. The synthesized polymer also shows visible light absorbance and also good oxygen evolution reaction at relatively low overpotentials, which is found to be better than other carbonaceous materials as well as metal oxides such as IrO_2. Thus, based on the current work, it is envisaged that porous polymers with adjustable bandgap can be developed using this technique which can have applications in catalysis, energy storage and biology.

Experimental

1-hexyl-3-methylimidazolium tris(pentafluoroethyl)trifluorophosphate [HMIM]FAP (HMIMFAP) was purchased in the highest available quality from Merck (Germany) and was used after drying under vacuum at 100 ^oC to remove the water content to below 2 ppm. Benzene (99.8%) and thiophene (>99%) were obtained from Sigma. Au, Pt and copper plates were used as the working electrodes. Au and Pt electrodes were cleaned under a hydrogen flame prior to the experiment. Copper was cleaned inside an XPS chamber by Ar ion sputtering until the spectrum

https://mc04.manuscriptcentral.com/jes-ecs

Accepted Manuscript For Review Only

showed only Cu signals. This was then transferred directly into the glove box which is connected to the XPS chamber and the electrochemical experiments were performed immediately. For Cu_xO substrates, the cleaned copper from the XPS chamber was introduced into the glove box which had an O_2 and H_2O concentration of 0.5ppm. The copper was then kept in the glove box for various times in order to produce a surface oxide layer after which the electropolymerization experiments were performed. The XPS of Cu and Cu_xO are shown in figure S13. Platinum wires were used as counter and quasi-reference electrodes (QRE) which were heated in a hydrogen flame to remove any surface impurities. The electrochemical cell was made of PTFE and clamped over a PTFE-covered Viton® O-ring onto the substrate, providing a geometric surface area of 0.3 cm^2. The Teflon cell and the O-ring were cleaned in a mixture of 50:50 vol% of concentrated H_2SO_4 and H_2O_2 (35%) followed by refluxing in distilled water.

The electrochemical measurements were performed in an argon-filled glove-box with water and oxygen contents of below 0.5 ppm (OMNI-LAB from Vacuum Atmospheres) by using a VersaStat III (Princeton Applied Research) potentiostat/galvanostat controlled by Versastudio software. The scan rate during cyclic voltammetry was set to 10 mV sec^{-1}. For polymer deposition, cyclic voltammetry was performed for 10 cycles between the open circuit potential and 2.3 V vs Pt. For the synthesis of bicontinuous polymer on Cu_xO, a potential of 1.5 V vs Pt was first applied for 10 minutes followed by running 10 CV cycles between OCP and 2.3 V. For the hydrogen evolution reaction, a three-electrode setup was used with the conducting polymer as the working electrode, saturated calomel electrode (SCE) as the reference electrode and carbon as the counter electrode. The effect of visible light on the HER was evaluated by illuminating the working electrode with a 50 mW blue LED having a wavelength between 460 and 480 nm. The potentials were not iR compensated. The potentials were converted to a reversible hydrogen electrode (RHE) scale using E(RHE)= 0.241 + 0.059×pH. For SEM (JEOL JSM7610F) and EDX analysis, the deposited polymer electrodes were cleaned with isopropanol overnight before the measurement.

X-ray Photoelectron spectra (XPS) were obtained using an ultrahigh vacuum (UHV) apparatus with a base pressure below $1x10^{-10}$ hPa. The sample was irradiated using the Al Kα line (photon energy of 1486.6 eV) of a non-monochromatic X-ray source (Omicron DAR 400). Electrons emitted were detected by a hemispherical analyser (Omicron EA125) under an angle of 45° normal to the surface with a resolution of 0.83 eV for detail spectra and 2.07 eV for survey

https://mc04.manuscriptcentral.com/jes-ecs

Accepted Manuscript For Review Only

spectra, respectively. All XPS spectra were displayed as a function of the binding energy with respect to the Fermi level.

Fourier transform infrared spectroscopy (VERTEX 70 V, Bruker Optics GmbH) with an attached attenuated total reflectance (ATR) module was used to characterise the polymer. The UV visible spectra was measured using a Cary 1100 UV-Vis-IR spectrometer**.**

AFM Force curves were collected using a Molecular Imaging Pico Plus AFM in contact mode. A silicon SPM-sensor from Nano World was employed for all experiments presented in this study. The spring constant was 6 N/m. All force curves were acquired at room temperature in an argon-filled glove box.

Computational details

Spin polarized periodic density functional theory (DFT) based calculations are performed using Vienna Ab Initio Simulation Package (VASP).[35, 36] The projector augmented wave (PAW) method is used and a cut-off energy of 550 eV is used for the expansion of the plane-wave basis sets, which gave bulk energies converged to within 10^{-5} eV.[37] The Perdew-Burke-Ernzerhof (PBE) version of generalized gradient approximation (GGA) is used to carry out the geometrical relaxation and the total energy calculations.[38] In this study we have also employed Grimme's dispersion correction (DFT+D3) as dispersive effects might be significant for these systems.[39]

The ideal Cu(111) surface is modelled by a 4x4 cell with 5 atomic layers from a bulk Cu with lattice parameter of 3.571 Å (Exp = 3.615 Å).[40] These calculations are performed using 5x5x1 k-points. The adsorption properties of benzene on Cu_2O(111) surface are investigated by considering a 3x3 cell with 7 atomic layers from a bulk Cu_2O with lattice parameter of 4.231 Å (Exp = 4.270 Å). In these calculations we employ DFT with Hubbard correction (DFT+U) using the Dudarev formalism and a U value of 6 eV, as reported in the previous studies, is used.[41, 42] All these calculations on Cu_2O(111) surface are performed using 3x3x1 k-points.

In the Cu(111) and Cu_2O(111) models, the adsorption of benzene is allowed only on one of the two exposed surfaces and the spurious dipole moment due to such adsorption is taken into account by using the methods implemented in VASP according to the procedures of Markov *et al.* and Neugebauer et al.[43, 44] In the direction perpendicular to the surface a vacuum gap of ~15 Å

Accepted Manuscript For Review Only

is used in order to eliminate the slab-slab interactions. In the Cu(111) surface and Cu_2O(111) surface three and four bottom atomic layers respectively are fixed to mimic the bulk of these systems.

Acknowledgment

We thank Mr Guozhu Li for XPS measurements. We acknowledge the use of Athena at HPC Midlands+ in this research, which was funded by the EPSRC (grant EP/P020232/1) via the EPSRC RAP call of spring 2018 and 2019. Supercomputer Wales is also thanked for the computing time. In this work ARCHER - the UK National Supercomputing Service (http://www.archer.ac.uk) was also used via the membership of the UK's HEC Materials Chemistry Consortium, which is funded by EPSRC (EP/L000202).

References

1. Böltau, M.; Walheim, S.; Mlynek, J.; Krausch, G.: Steiner, U. Surface-Induced Structure Formation of Polymer Blends on Patterened Substrates. *Nature*, **1998**, 391, 877-879
2. Tsurusawa, H.: Russo, J.; Leocmach, M.; Tanaka, H. Formation of Porous Crystals via Viscoelastic Phase Separation. *Nat. Mater.*, **2017**, 16, 1022-1028
3. Seo, M.; Hillmyer, M. A. Reticulated Nanoporous Polymers by Controlled Polymerization-Induced Microphase Separation. *Science*, **2012**, 336, 1422-1425
4. Xue, L.; Zhang, J.; Han, Y. Phase Separation Induced Ordered Patterns in Thin Polymer Blend Films. *Prog. Polymer. Sci.*, **2012**, 37, 564-594
5. Winesaft, D. A.; Ade, H.; Sokolov, J.; Rafailovich, M.; Zhu, S. Substrate Dependance of Morphology in Thin Film Polymer Blends of Polystyrene and Poly(methyl methacrylate). *Polym. Int.*, **2000**, 49, 458-462
6. Resel, R. Surface Induced Crystallographic Order in Sexiphenyl Thin Films. *J. Phys.: Condens. Matter.*, **2008**, 20, 184009/1-184009/10
7. Winkler, A. On the Nucleation and Initial Film Growth of Rod-Like Organic Molecules. *Surf. Sci.*, **2016**, 652, 367-377
8. Jenekhe, S. A.; Chen, X. L. Self-Assembly of Ordered Microporous Materials from Rod-Coil Block Copolymers. *Science*, **1999**, 283, 372-375

Accepted Manuscript
For Review Only

9. Coakley, K. M.: Liu, Y.; McGehee, M. D.; Frindell, K. L.; Stucky, G. D. Infiltrating Semiconducting Polymer into Self-Assembled Mesoporous Titania Films for Photovoltaic Applications. *Adv. Func. Mater.*, **2003**, 13, 301-306
10. Wu, D.: Xu, F.; Sun, B.; Fu, R.; He, H.; Matyajaszewski, K. Design and Preparation of Porous Polymers. *Chem. Rev.*, **2012**, 112, 3959-4015
11. Han, J.; Song, G.; Guo, R. A Facile Solution Route for Polymeric Hollow Spheres with Controllable Size. *Adv. Mater.*, **2006**, 18, 3140-3144
12. Krausch, G. Surface Induced Self Assembly in Thin Polymer Films. *Mater. Sci. Eng. R.*, **1995**, 14, 1-94
13. Novák, J.; Oehzelt, M.; Berkebile, S.; Koini, M.; Ules, T.; Koller, G.; Haber, T.; Resel, R.; Ramsey, M. G. Crystal Growth of Para-Sexiphenyl on Clean and Oxygen Reconstructed Cu(110) Surfaces. *Phys. Chem. Chem. Phys.*, **2011**, 13, 14675-14684
14. Wagner, M.; Berkebile, S.; Netzer, F. P.; Ramsey, M. G. Revelaing the Buried Metal-Organic Interfae: Restructuring of the First Layer by van der Waals Forces. *ACS Nano*, **2015**, 9, 12070-12078
15. Villarreal, I.; Morales, E.; Otero, T. F.; Acosta, J. L. Electropolymerization Kinetics of Pyrrole in Aqueous Solution on Graphite Felt Electrodes. *Synthetic Metals.*, **2001**, 123, 487-492
16. Bhadani, S. N.; Parravano, G. Electrochemical Anionic Polymerization of 4-Vinylpyridine in Pyridine. *J. Poly. Sci.*, **1970**, 8, 225-235
17. Lahiri, A.; Behrens, N.; Pulletikurthi, G.; Yochelis, A.; Kroke, E.; Cui, T.; Endres, F. Electrochemically Induced Phase Separation and In Situ Formation of Mesoporous Structures in Ionic Liquid Mixtures. *Sci. Adv.*, **2018**, 4, eaau9663
18. Lacaze, P. C.; Hara, S.; Soubiran, P.; Aeiyach, S. Structure and Growth Mechanims of Polyphenylene Films Formed on Platinum by Anodic Polymerization of Benzene and Biphenyl in Various Electrolytic Media. *Synth. Metals.*, **1995**, 75, 111-118
19. Delamar, M.; Lacaze, P. C.; Lemiere, B.; Dumousseau, J. Y.; Dubois, J. E. A New Method for Preparing Polysulfones: Electrochemically Induced Copolymerization of Sulfur Dioxide and Conjugated Dienes in Liquid SO_2. *J. Polym. Sci. Polym. Chem.* **1982**, 20, 245
20. Lerner, N. R. ESR and Chemical Study of p-Polyphenylene formed by using an $AlCl_3$-$CuCl_2$ Catalyst. *J. Polym. Sci. Polym. Chem*. **1974**, 12, 2477

https://mc04.manuscriptcentral.com/jes-ecs

Accepted Manuscript For Review Only

21. Aeiyach, S.; Soubiran, P.; Lacaze, P. C. Influence of the Temperature on the Structure of Poly(p-phenylene) (PPP) Films Formed by Electropolymerization of Benzene on Platinum Electrodes in Sulphur Dioxide Medium. *Polym. Commun.* **1988**, 29, 130
22. Havinga, E. E.; Van Horssen, L. W. Dependence of the Electrical Conductivity of Heavily-Doped Poly-p-Phenylenes on the Chain Length. *Synth. Met.* **1986**, 16, 55–70
23. Shacklette, L. W.; Eckhardt, H.; Chance, R. R.; Miller, G. G.; Ivory, D. M.; Baughman, R. H. Solid-State Synthesis of Highly Conducting Polyphenylene from Crystalline Oligomers. *J. Chem. Phys.*, **1980**, 73, 4098-4102
24. Lére-Porte, J. P.; Radi, M.; Choro, C.; Petrissans, J.; Sauvajol, J. L.; Gonbeau, D.; Pfister-Guillouzo, G.; Louarn, G.; Lefrant, S. Characterization from XPS, FTIR and Raman Spectroscopies of Films of Poly(p-Phenylene) Prepared by Electropolymerization of Benzene Dissolved in Ketyl Pyridinium Chloride-$AlCl_3$ Melt. *Synthetic Metals*, **1993**, 59, 141-149
25. Gardella, A. J.; Ferguson, S. A.; Chin, R. L. $\pi^* \leftarrow \pi$ Shakeup Satellites for the Analysis of Structure and Bonding in Aromatic Polymers by X-ray Photoelectron Spectroscopy. *Appl. Spectroscopy.*, **1986**, 40, 224-232
26. Tian, W. J.; Zhang, H. Y.; Shen, J. C. Some Properties of Interfaces Between Metals and Polymers. *Surf. Rev. Lett.*, **1997**, 4, 703-708
27. Nguyen, T. P.; Ettaik, H.; Lefrant, S.; Leising, G.; Stelzer, F. Studies of the Polyparaphenylene/Aluminium Interface. *Synth. Metals.*, **1990**, 38, 69-76
28. Lögdlund, M.; Brédas, J. L. Theoritical Studies on the Interaction Between Aluminium and Poly(p-phenylenevinylene) and Derivatives. *J. Chem. Phys.*, **1994,** 101, 4357-4364
29. Mulazzi, E.; Ripamonti, A.; Athouël, L.; Wery. J.; Lefrant, S. Theoretical and Experimental Investigation of the Optical Properties of Poly(Paraphenylene): Evidence of Chain-Length Distribution. *Phys. Rev. B.*, **2002**, 65, 085204/1-085204/9
30. Shao, M.: He, Y.; Hong, K.; Rouleau, C. M.; Geohegan, D. B.; Xiao, K. A Water-Soluble Polythiophenefor Organic-Field Transistors. *Poly. Chem.*, **2013**, 4, 5270-5274
31. Clément, S.; Tizit, A.; Desbief, S.; Mehdi, A.; De Winter, J.; Gerbaux, P.; Lazzaroni, R.; Boury, B. Synthesis and Characterization of π-Conjugated Polymer/Silica Hybrids Containing Regioregular Ionic Polythiophenes. *J. Mater. Chem.*, **2011**, 21, 2733-2739
32. Chen, S.; Duan, J.; Ran, J.; Qiao, S. Z. Paper-Based N-Doped Carbon Films for Enhanced Oxygen Evolution Electrocatalysis. *Adv. Sci.*, **2015**, 2, 1400015

Accepted Manuscript For Review Only

33. Carstens, T.; Zein El Abedin, S.; Endres, F. Electrosynthesis of Poly (Para) Phenylene in and Ionic Liquid: Cyclic Voltammetry and In Situ STM/Tunneling Spectroscopy Studies. *ChemPhysChem*, **2008**, 9, 439-444
34. Lai, J.; Nsabimana, A.; Luque, R.; Xu, G. 3D Porous Carbonaceous Electrodes for Electrocatalytic Applications. *Joule*, **2018**, 2, 76-93
35. Kresse, G.; Hafner, J. Ab Initio Molecular Dynamics for Liquid Metals. *Phys. Rev. B.*, **1993**, 47, 558-561
36. Kresse, G.; Hafner, J. Ab Initio Molecular-Dynamics Simulation of the Liquid-Metal-Amorphous-Semiconductor Transition in Germanium. *Phys. Rev. B.*, **1994**, 49, 14251-14269
37. Blöchl, P. E. Projector Augmented-Wave Method. *Phys. Rev. B.*, **1994**, 50, 17953-17979
38. Perdew, J. P.; Burke, K.; Ernzerhof, M. Generalized Gradient Approximation Made Simple. *Phys. Rev. Lett.*, **1996**, 77, 3865-3868
39. Grimme, S.; Antony, J.; Ehrlich, S.; Krieg, H. A Consistent and Accurate Ab Initio Parametrization of Density Funtional Dispersion Correction (DFT-D) for the 94 Elements H-Pu. *J. Chem. Phys.*, **2010,** 132, 154104
40. Chutia, A.; Silverwood, I. P.; Farrow, M. R.; Scanlon, D. O.; Wells, P. P.; Bowker, M.; Parker, S. F.; Catlow, C. R. A. Adsorption of Formate Species on Cu(h,k,l) Low Index Surfaces. *Surf. Sci.*, **2016**. 653, 45-54
41. Bendavid, L. I.; Carter, E. A. CO_2 Adsorption on Cu_2O(111): A DFT+U and DFT-D Study. *J. Phys. Chem. C*, **2013**, 117, 26048–26059
42. Nie, X.; Griffin, G. L.; Janik, M. J.; Asthagiri, A. Surfaces Phases of Cu_2O(111) Under CO_2 Electrochemical Reduction Conditions. *Catal. Commun.*, **2014**, 52, 88–91
43. Makov, G.; Payne, M. Periodic Boundary Conditions in Ab Initio Calculations. *Phys. Rev. B.*, **1995**, 51, 4014–4022
44. Neugebauer, J.; Scheffler, M. Adsorbate-Substrate and Adsorbate-Adsorbate Interactions of Na and K Adlayers on Al (111). *Phys. Rev. B.*, **1992**, 46, 16067–16080

Accepted Manuscript
For Review Only